Phase Diagram and Superconducting Dome of Infinite-Layer $Nd_{1-x}Sr_xNiO_2$ Thin Films

Shengwei Zeng [1,2,*], Chi Sin Tang, [1,3,4] Xinmao Yin, [1,4] Changjian Li, [2,5] Mengsha Li, [5] Zhen Huang, [2] Junxiong Hu, [1,2] Wei Liu, [1] Ganesh Ji Omar [1,2] Hariom Jani [2,3] Zhi Shiuh Lim, [1,2] Kun Han, [2] Dongyang Wan [1,2] Ping Yang, [4] Stephen John Pennycook, [2,5] Andrew T. S. Wee, [1,3,4,6] and Ariando Ariando [1,2,3,6,†]

[1]*Department of Physics, Faculty of Science, National University of Singapore, Singapore 117551, Singapore*
[2]*NUSNNI-NanoCore, National University of Singapore, Singapore 117411, Singapore*
[3]*NUS Graduate School for Integrative Sciences and Engineering, National University of Singapore, Singapore 117456, Singapore*
[4]*Singapore Synchrotron Light Source (SSLS), National University of Singapore, Singapore 117603, Singapore*
[5]*Department of Materials Science and Engineering, National University of Singapore, Singapore 117575, Singapore*
[6]*Centre for Advanced 2D Materials and Graphene Research, National University of Singapore, Singapore 117546, Singapore*

Infinite-layer $Nd_{1-x}Sr_xNiO_2$ thin films with Sr doping level x from 0.08 to 0.3 are synthesized and investigated. We find a superconducting dome x between 0.12 and 0.235 accompanied by a weakly insulating behavior in both under- and overdoped regimes. The dome is akin to that in the electron-doped 214-type and infinite-layer cuprate superconductors. For $x \geq 0.18$, the normal state Hall coefficient (R_H) changes the sign from negative to positive as the temperature decreases. The temperature of the sign changes decreases monotonically with decreasing x from the overdoped side and approaches the superconducting dome at the midpoint, suggesting a reconstruction of the Fermi surface with the dopant concentration across the dome.

The recent discovery of superconductivity in doped infinite-layer nickelate $Nd_{0.8}Sr_{0.2}NiO_2$ thin films has hailed another milestone in the field of high-temperature superconductivity [1]. In contrast to the antiferromagnetic (AF) order in the cuprates, the parent compound $NdNiO_2$ shows no sign of magnetic order down to a temperature of 1.7 K [2], despite its similarities in the crystalline and electronic structures to the high-T_c cuprates. This severely challenges the scenario of AF spin fluctuation as the superconducting pairing mechanism, which is prevalent in the cuprates [3–5]. The nickelate may represent a new type of superconductivity and has motivated numerous theoretical works to explore the similarities and differences of the cuprates [6–25]. Among the similarities are the large value of the $RNiO_2$ (R = La, Nd) long-range hopping t' and the e_g energy splitting [6] and the possible d-wave pairing symmetry as suggested by the t-J model [12,13]. It has been proposed, however, that the coupling between the low-density Nd-$5d$ conduction electrons and the localized Ni-$3d$ electron forms Kondo spin singlets and thus suppresses the long-range AF order [15]. Further, while the doped holes in the $Nd_{1-x}Sr_xNiO_2$ reside at the Ni sites, they are at the oxygen sites in the cuprates due to the strong hybridization of the Cu-$3d_{x2-y2}$ and O-$2p$ orbitals [11,14]. The role of the Nd $4f$ state in $NdNiO_2$, which shows no substantial effect in cuprates, has also been considered [7,10].

Experimentally, x-ray spectroscopy suggests a weakly interacting three-dimensional $5d$ metallic state in the rare-earth spacer layer hybridizing with the strongly correlated $3d_{x2-y2}$ state in the NiO_2 layer [26]. Spin fluctuations in bulk $NdNiO_2$ have been explored by Raman spectroscopy, which suggested an AF exchange of $J = 25$ meV [27]. $Nd_{1-x}Sr_xNiO_2$ ($x = 0$, 0.2, 0.4) prepared in bulk form shows the absence of superconductivity even under 50.2 GPa pressure, probably due to the creation of nickel deficiency during the reduction process [28]. Additionally, attempts in growing the nickelate infinite-layer films at low oxygen partial pressure without chemical reduction have resulted in insulating thin films [29]. It is clear that the synthesis of the superconducting nickelate is challenging and critical.

One important feature in most unconventional superconductors is that the superconductivity is induced by charge doping in the parent compound. Variation in the dopant concentration leads to a phase diagram in which a superconducting (SC) dome is embedded within other competing ordered phases, such as insulator and metal [30,31]. For the isostructural cuprates, increasing charge doping causes transitions from a Mott insulating to a high-T_c superconducting and then a Fermi liquid metallic state [30]. It is important to note here that the use of the Nd atom and the $x = 0.2$ value in the $Nd_{0.8}Sr_{0.2}NiO_2$ superconductor has been inspired by the need to achieve a higher conductivity in the $La_{0.8}Sr_{0.2}NiO_2$ through substituting the La with a smaller ionic radius atom Nd and thus increasing the electronic bandwidth [1]. In contrast to the expectation of hole doping by Sr, the normal state R_H of the

$Nd_{0.8}Sr_{0.2}NiO_2$ showed a negative sign at room temperature. However, whether the superconducting and normal state properties in $Nd_{1-x}Sr_xNiO_2$ are doping dependent thus far remains unresolved [32]. In this Letter, we report the synthesis of the infinite-layer $Nd_{1-x}Sr_xNiO_2$ with different Sr doping levels showing a SC dome for $0.12 < x < 0.235$ with a weak insulating state in both the under- and overdoped regimes beside the dome. The overdoped regime behaves differently from the high-T_c cuprates, wherein Fermi liquid metal behavior is seen.

The ceramic targets were prepared by sintering the mix of the Nd_2O_3, $SrCO_3$, and NiO powder (weighted according to the chemical formula of $Nd_{1-x}Sr_xNiO_3$) in the air for 15 h at 1200, 1220, and 1250 °C, respectively, with a regrinding process before each sintering. For the final sintering at 1250 °C, the powder was pressed into a disk-shaped pellet. Thin films with a thickness of ~35 nm (unless otherwise indicated) were grown on a TiO_2-terminated (001) $SrTiO_3$ (STO) substrate using a pulsed laser deposition (PLD) technique with a 248-nm KrF excimer laser. The nominal composition of the as-grown thin films is assumed to be the same as the target. No capping layer is introduced for all samples in this study. The deposition temperature and oxygen partial pressure P_{O2} for all samples were 600 °C and 150 mTorr, respectively. The laser energy density on the target surface was set to be 2 J cm^{-2}. After deposition, the samples were cooled down to room temperature at a rate of 8 °C/ min at deposition pressure. It has been suggested that, to induce a superconducting phase, the infinite-layer nickelate needs to be chemically reduced by annealing the sample and CaH_2 powder in a vacuum that stimulates the H_2 gas-phase reaction with the sample [1,2,33–35]. In our case, we performed this chemical reduction in the PLD vacuum chamber after cutting the samples into pieces of size around 1.3×2.5 mm^2 and wrapping them in an aluminum foil together with about 0.1 g of CaH_2 powder (the samples were embedded in CaH_2 powder). During the reduction process, the samples were heated up to 340–360 °C at a rate of 25 °C/ min, kept at that temperature for 80–120 min, and then cooled down to room temperature at a rate of 25 °C/ min. We note here that the pressure changed from the background of 1×10^{-5} to around 1×10^{-1} Torr during the heating, which was then maintained during the whole reduction process. The increase in pressure may be caused by the release of H_2 gas upon CaH_2 heating and/or H_2O gas due to a chemical reaction between the sample and CaH_2 [36]. The x-ray diffraction (XRD) measurement was done in the x-ray diffraction and development beam line at Singapore Synchrotron Light Source with an x-ray wavelength of $\lambda = 1.5404$ Å. The wire connection for the electrical transport measurement was made by Al ultrasonic wire bonding. The transport measurements were performed using a quantum design physical property measurement system. The high-angle annular dark-field scanning transmission electron microscopy (HAADF-STEM) imaging was carried out at 200 kV using a JEOL ARM200F microscope and the cross-sectional TEM specimens were prepared by a focused ion beam machine (FEI Versa 3D).

Figure 1 depicts the XRD θ-2θ patterns of the $Nd_{1-x}Sr_xNiO_2$ thin films with a Sr doping level x from 0.08 to 0.3 after the chemical reduction, showing only the (00l) infinite-layer peaks (l is an integer), which is consistent with a transformation of the $Nd_{1-x}Sr_xNiO_3$ from a perovskite to an infinite-layer structure. The thin film peaks also slightly shift toward a lower angle as x increases, indicating an expansion of the c-axis lattice constants d from 3.30 Å at $x = 0.08$ to 3.42 Å at $x = 0.3$, as plotted in the inset of Fig. 1. This result is in agreement with the empirical expectation when replacing the cation with an atom having a larger ionic radius. The full width at half maximum of the rocking curves for the (002) peaks shows a value between 0.05° and 0.11°, indicating a good quality of the infinite-layer film (Fig. S1 in the Supplemental Material) [37]. The structural characterization of the as-grown $Nd_{1-x}Sr_xNiO_3$ thin films can be found in Fig. S2 [37] for comparison.

Figure 2 shows the resistivity versus temperature (ρ-T) curves of the $Nd_{1-x}Sr_xNiO_2$ thin films for x from 0.08 to 0.3. For $0.08 \leq x \leq 0.12$, the samples show a metallic behavior at high temperatures with a resistivity minimum between 27 and 35 K, below which a weakly insulating behavior is seen. For $0.135 \leq x \leq 0.22$, the samples are superconducting and the ρ-T curves behave like a metal above the superconducting
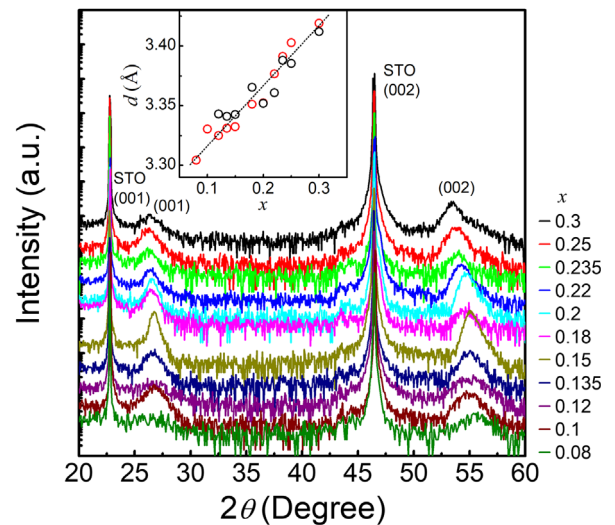

FIG. 1. The XRD θ-2θ scan patterns of the $Nd_{1-x}Sr_xNiO_2$ thin films on a STO substrate. The intensity is vertically displaced for clarity. The inset shows room-temperature c-axis lattice constants d as a function of Sr doping level x. The red circles represent the data extracted from the θ-2θ scans in Fig. 1 and the black circles represent another set of samples at each doping level for $0.12 \leq x \leq 0.3$. The dashed line in the inset is a guide to the eye. The measurements were done at room temperature.
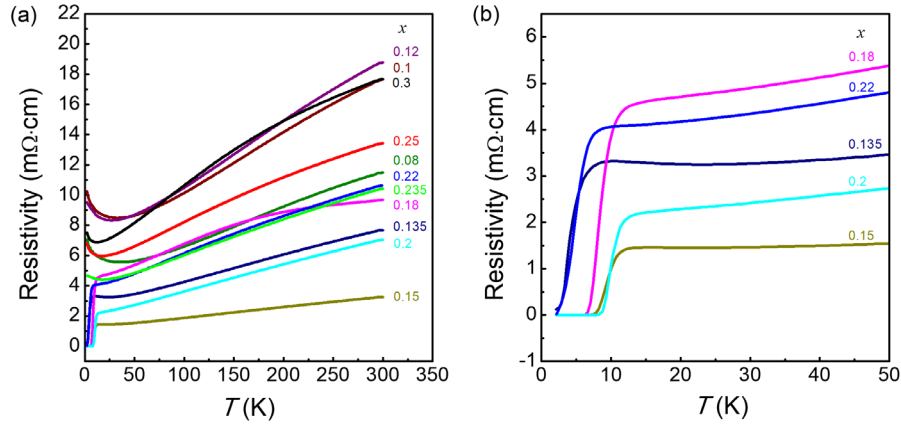
FIG. 2. (a) The resistivity versus temperature (ρ-T) curves of the $Nd_{1-x}Sr_xNiO_2$ thin films with Sr doping level x from 0.08 to 0.3. (b) The enlarged ρ-T curves at temperatures from 50 to 2 K for the superconducting $Nd_{1-x}Sr_xNiO_2$ with x from 0.135 to 0.22.

transition temperature. Figure 2(b) shows the enlarged ρ-T curves near the superconducting transition temperatures for $0.135 \leq x \leq 0.22$. For the higher doping levels $x \geq 0.235$, the resistivity behavior is similar to the underdoped ones but with a minimum between 12 and 18 K. The weakly insulating behavior at low temperature in unconventional superconductors has also been observed in underdoped cuprates and attributed to the localization and/or Kondo effect [38,39]. In nickelates, a theoretical calculation has suggested the Kondo effect to explain the resistance upturn in undoped $LaNiO_2$ and $NdNiO_2$ [15]. With Sr doping in $Nd_{1-x}Sr_xNiO_2$, both the under- and overdoped sides also show such a resistance upturn, the origin of which needs further investigation. To further confirm the emergence of the superconductivity, we demonstrate a suppression of the T_c with magnetic fields in the ρ-T curves for $x = 0.2$, as shown in Fig. S3 [37]. The ρ-T curves of the as-grown $Nd_{1-x}Sr_xNiO_3$ and additional $Nd_{1-x}Sr_xNiO_2$ samples for $x = 0.12$–0.3 films can be found in Figs. S4 and S5 [37], respectively, signifying the reproducibility of the samples and the importance of the reduction process.

Figure 3(a) shows the temperature dependence of the normal state R_H for the $Nd_{1-x}Sr_xNiO_2$ films. At room temperature, the R_H of all samples shows a negative sign and its magnitude ($|R_H|$) decreases with increasing x and then saturates at $x > 0.2$ [Fig. 3(b)]. This R_H behavior indicates that the charge carriers are electrons with a density increasing with x (considering the carrier density $n = 1/eR_H$, where e is the electron charge), in contrast to the expectation of a single-band hole doping as a result of the Nd-by-Sr substitution. While the R_H remains negative below 300 K for samples with $x \leq 0.15$, it becomes positive at low temperature for samples with $x \geq 0.18$. Figure 3(b) presents the doping dependence of the R_H at 20 K, clearly showing a sign change at $x = 0.15$–0.18 from negative to positive with increasing x. For the samples with $x \leq 0.135$, the $|R_H|$ increases moderately with decreasing the temperature (down to 100–200 K depending on x) and then decreases again with further decrease of the temperature. This behavior is similar to the observation in both electron-doped $Pr_{2-x}Ce_xCuO_4$ and hole-doped $La_{2-x}Sr_xCuO_4$ cuprates [40–42]. For samples with $x = 0.15$, the $|R_H|$ decreases monotonically as the temperature is reduced.

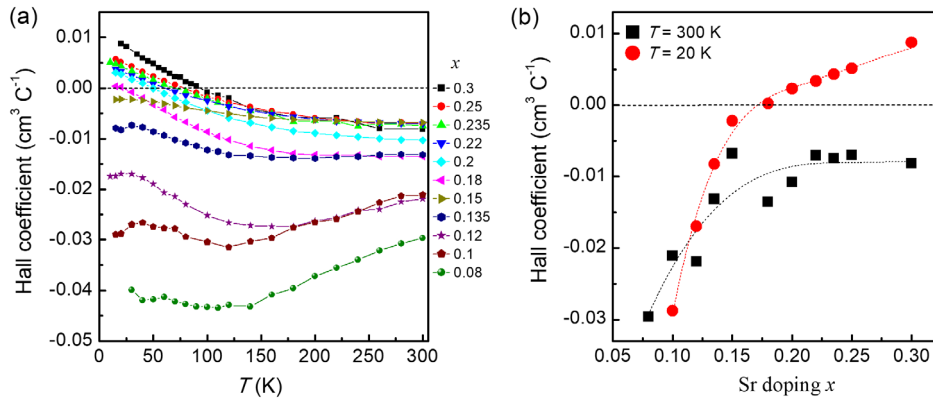FIG. 3. (a) The temperature dependence of the R_H for the $Nd_{1-x}Sr_xNiO_2$ thin films with a Sr doping level x from 0.08 to 0.3. (b) The R_H at $T = 300$ and 20 K as a function of x. The dashed lines are guides to the eye.

For samples with $x \geq 0.18$, the $|R_H|$ decreases with decreasing temperature at the negative side and increases at the positive side. This indicates cancellation of the electron and hole contribution as the temperature decreases for those samples. Even though the electron density is higher (lower $|R_H|$) at a higher Sr doping level, the hole contribution is much more obvious, leading to a higher temperature where the R_H changes from negative to positive sign (denoted as T_H) at higher x (Fig. 4).

Even though the room-temperature electron density generally increases with x, the ρ does not follow a similar trend at the overdoped regime $x \geq 0.235$ (Fig. 2). In addition, the ρ and $|R_H|$ of our thin films are higher than those in previous reports [1,32]. These could be due to the higher temperature (340–360 °C) of the reduction process in our experiment. Indeed, previous results showed that the resistivity of the LaNiO₂ increased with increasing reduction temperature even though the films showed similar infinite-layer XRD peaks [36]. The possibility of having more intercalating hydrogen at a higher reduction temperature may also influence the ρ and $|R_H|$, as theoretically predicted in Ref. [43]. As the film thickness increases, moreover, the Ruddlesden-Popper–type phase can emerge, as can be seen from the HAADF-STEM image (Fig. S6 in the Supplemental Material) [33,37], which may also cause
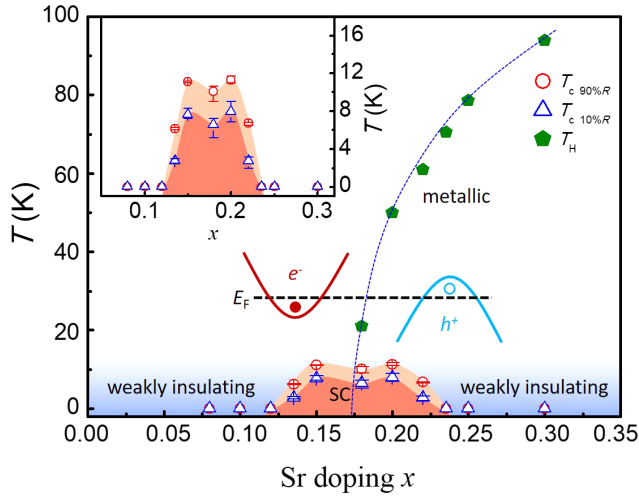

FIG. 4. The critical temperature T_c and temperature where the R_H changes from negative to positive sign T_H. The $T_{c90\%R}$ ($T_{c10\%R}$) are defined to be the temperature at which the resistivity drops to 90% (10%) of the value at 15 K (the onset of the superconductivity). The red circles and blue triangles represent the average T_c of the samples shown in Fig. 2 and Fig. S5 [37]. The error bars represent the T_c variation. The T_H is defined to be the temperature at which the R_H curve crosses the axis at zero in Fig. 3. The blue dashed line is a guide to the eye. The inset in the left upper corner is the enlarged view of the SC dome. The inset at the bottom schematically shows the electron band (e^-) and hole band (h^+), which dominate the charge carriers in the two panels separated by the T_H-x curve. The black dashed line in the inset is the Fermi energy (E_F).

an increase in the ρ. Even though there exists a variation in ρ due to the difference in the thickness and reduction temperature, the superconductivity and the superconducting transition temperature are reproducible and robust for different dopant levels. The resultant phase diagram is therefore conclusive.

Figure 4 depicts a phase diagram of the Nd₁₋ₓSrₓNiO₂ showing a SC dome of $0.12 < x < 0.235$, consistent with that in a recent report [32]. The SC dome of the Nd₁₋ₓSrₓNiO₂ is comparable to that of electron-doped cuprates Sr₁₋ₓLaₓCuO₂ and Pr₂₋ₓCeₓCuO₄ [44–46], which is much narrower compared to the hole-doped cuprate La₂₋ₓSrₓCuO₄ [47]. A small dip at the top of the SC dome was observed at $x = 0.18$, which is also visible in Ref. [32] but at $x = 0.2$. A similar feature has been observed in La₂₋ₓMₓCuO₄ ($M =$ Sr and Ba) at $x = 1/8$, which was ascribed to the presence of the charge stripe [47,48]. The T_H for the samples with $x \geq 0.18$ is also shown in the phase diagram in Fig. 4. As x decreases from the overdoped side, T_H decreases monotonically. A simplified two-band model with both electron- and holelike Fermi surfaces is shown schematically in the inset of Fig. 4. The T_H-x curve separates the normal state regime into two panels, with the right panel dominated by the holelike band and the left panel by the electronlike band. With decreasing the temperature and increasing the Sr concentration, the bands dominating the normal state electrical transport evolve from an electron- to a holelike band. Therefore, the R_H changes sign from negative to positive. It is worth noting that the extension of the T_H-x curve reaches the middle of the superconducting dome, suggesting a reconstruction of the Fermi surface as the doping changes across the middle point of the dome.

The two-band model can be captured by the Hall resistance R_{xy} as a function of magnetic field B [32,49,50]. Considering the opposite sign of the electron and hole carrier and $R_H = R_{xy}/B$, the R_H in the simple two-band model can be written as

$$R_H = \frac{1}{e} \frac{(n_h \mu_h^2 - n_e \mu_e^2) + (\mu_h \mu_e B)^2 (n_h - n_e)}{(n_h \mu_h + n_e \mu_e)^2 + (\mu_h \mu_e B)^2 (n_h - n_e)^2},$$

where n_e and n_h are the electron and hole density, μ_e and μ_h are the electron and hole mobility, respectively, and e is the elementary charge [32,49,50]. In a low-field limit, the R_H can be simplified as

$$R_H = \frac{1}{e} \frac{n_h \mu_h^2 - n_e \mu_e^2}{(n_h \mu_h + n_e \mu_e)^2}.$$

Therefore, the difference between the n_e and n_h and the temperature dependencies of the μ_e and μ_h cause the R_H sign changes with the doping and temperature, as observed in Figs. 3 and 4. This model predicts a nonlinearity in R_{xy} at

high fields and a fit to R_{xy} can provide an estimate to the density and mobility of both hole and electron carriers [49,50]. However, in our measurements, the R_{xy} shows a perfect linear behavior up to 9 T (Fig. S8 in the Supplemental Material) [37], which prevents us from quantitatively extracting the value of n_e and n_h. Nevertheless, the two-band model is consistent with the picture constructed by the electronic structure calculations, which show the hole pocket originating from a Ni-$3d_{x2-y2}$ orbital and the electron pockets from the rare-earth element $5d_{xy}$ and $5d_{3z2-r2}$ orbitals in the parent compound [6–8,23–26]. Moreover, upon hole doping, the $5d$ electron pocket diminishes and/or the new $3d$ hole pocket evolves, which may explain the observed sign change of the R_H as the Sr composition increases [6,24].

In summary, we have synthesized infinite-layer $Nd_{1-x}Sr_xNiO_2$ thin films with a doping level x from 0.08 to 0.3 and found a SC dome x between 0.12 and 0.235. In both under- and overdoped regimes adjacent to the dome, a weakly insulating behavior is observed, which is different from the high-T_c cuprates in which a Fermi liquid metal is seen in the overdoped regime. The width of the dome is comparable to that of the electron-doped infinite-layer $Sr_{1-x}La_xCuO_2$ and 214-type $Pr_{2-x}Ce_xCuO_4$. Finally, we have demonstrated a synthesis process of the infinite-layer nickelate thin films via a chemically topotactic reduction process in a sealed vacuum chamber, facilitating future studies of an *in situ* reaction by-product monitoring for better control of the reduction process.

---

[*]Corresponding author.
phyzen@nus.edu.sg
[†]Corresponding author.
ariando@nus.edu.sg

[1] D. Li, K. Lee, B. Y. Wang, M. Osada, S. Crossley, H. R. Lee, Y. Cui, Y. Hikita, and H. Y. Hwang, Superconductivity in an infinite-layer nickelate, Nature (London) **572**, 624 (2019).

[2] M. A. Hayward and M. J. Rosseinsky, Synthesis of the infinite layer Ni(I) phase $NdNiO_{2+x}$ by low temperature reduction of $NdNiO_3$ with sodium hydride, Solid State Sci. **5**, 839 (2003).

[3] P. W. Anderson, The resonating valence bond state in La_2CuO_4 and superconductivity, Science **235**, 1196 (1987).

[4] G. A. Sawatzky, Superconductivity seen in a non-magnetic nickel oxide, Nature (London) **572**, 592 (2019).

[5] R. M. Wilson, Superconductivity is found in a nickel oxide, Phys. Today **72**, No. 11, 19 (2019) .

[6] A. S. Botana and M. R. Norman, Similarities and Differences between $LaNiO_2$ and $CaCuO_2$ and Implications for Superconductivity, Phys. Rev. X **10**, 011024 (2020).

[7] P. Jiang, L. Si, Z. Liao, and Z. Zhong, Electronic structure of rare-earth infinite-layer $RNiO_2$ ($R =$ La, Nd), Phys. Rev. B **100**, 201106(R) (2019).

[8] F. Lechermann, Late transition metal oxides with infinite-layer structure: Nickelates versus cuprates, Phys. Rev. B **101**, 081110(R) (2020).

[9] Y. Nomura, M. Hirayama, T. Tadano, Y. Yoshimoto, K. Nakamura, and R. Arita, Formation of a two-dimensional single-component correlated electron system and band engineering in the nickelate superconductor $NdNiO_2$, Phys. Rev. B **100**, 205138 (2019).

[10] M.-Y. Choi, K.-W. Lee, and W. E. Pickett, Role of $4f$ states in infinite-layer $NdNiO_2$, Phys. Rev. B **101**, 020503(R) (2020).

[11] M. Jiang, M. Berciu, and G. A. Sawatzky, Critical Nature of the Ni Spin State in Doped $NdNiO_2$, Phys. Rev. Lett. **124**, 207004 (2020).

[12] X. Wu, D. Di Sante, T. Schwemmer, W. Hanke, H. Y. Hwang, S. Raghu, and R. Thomale, Robust $dx2 − y2$ -wave superconductivity of infinite-layer nickelates, Phys. Rev. B **101**, 060504(R) (2020).

[13] Y. H. Zhang and A. Vishwanath, Type II t–J model in superconducting nickelate $Nd_{1-x}Sr_xNiO_2$, Phys. Rev. Research **2**, 023112 (2020).

[14] H. Zhang, L. Jin, S. Wang, B. Xi, X. Shi, F. Ye, and J. W. Mei, Effective Hamiltonian for nickelate oxides $Nd_{1-x}Sr_xNiO_2$, Phys. Rev. Research **2**, 013214 (2020).

[15] G.-M. Zhang, Y.-f. Yang, and F.-C. Zhang, Self-doped Mott insulator for parent compounds of nickelate superconductors, Phys. Rev. B **101**, 020501(R) (2020).

[16] J. E. Hirsch and F. Marsiglio, Hole superconductivity in infinite-layer nickelates, Physica (Amsterdam) **566C**, 1353534 (2019).

[17] S. Ryee, H. Yoon, T. J. Kim, M. Y. Jeong, and M. J. Han, Induced magnetic two-dimensionality by hole doping in the superconducting infinite-layer nickelate $Nd_{1-x}Sr_xNiO_2$, Phys. Rev. B **101**, 064513 (2020).

[18] L.-H. Hu and C. Wu, Two-band model for magnetism, and superconductivity in nickelates, Phys. Rev. Research **1**, 032046(R) (2019).

[19] F. Bernardini, V. Olevano, and A. Cano, Magnetic penetration depth and T_c in superconducting nickelates, Phys. Rev. Research **2**, 013219 (2020).

[20] Y. Gu, S. Zhu, X. Wang, J. Hu, and H. Chen, A substantial hybridization between correlated Ni-d orbital and itinerant

electrons in infinite-layer nickelates, Commun. Phys. **3**, 1 (2020).

[21] M. Kitatani, L. Si, O. Janson, R. Arita, Z. Zhong, and K. Held, Nickelate superconductors—A renaissance of the one-band Hubbard model, npj Qauntum Mater. **5**, 59 (2020).

[22] J. Karp, A. S. Botana, M. R. Norman, H. Park, M. Zingl, and A. Millis, Many-Body Electronic Structure of NdNiO$_2$ and CaCuO$_2$, Phys. Rev. X **10**, 021061 (2020).

[23] H. Sakakibara, H. Usui, K. Suzuki, T. Kotani, H. Aoki, and K. Kuroki, Model Construction and a Possibility of Cuprate-Like Pairing in a New d^9 Nickelate Superconductor (Nd, Sr)NiO$_2$, Phys. Rev. Lett. **125**, 077003 (2020).

[24] J. Gao, Z. Wang, C. Fang, and H. Weng, Electronic structures and topological properties in nickelates Ln$_{n+1}$Ni$_n$O$_{2n+2}$, Nat. Sci. Rev. (2020), https://doi.org/10.1093/nsr/nwaa218.

[25] Z. Liu, Z. Ren, W. Zhu, Z. Wang, and J. Yang, Electronic and magnetic structure of infinite-layer NdNiO$_2$: Trace of antiferromagnetic metal, npj Quantum Mater. **5**, 1 (2020).

[26] M. Hepting *et al.*, Electronic structure of the parent compound of superconducting infinite-layer nickelates, Nat. Mater. **19**, 381 (2020).

[27] Y. Fu, L. Wang, H. Cheng, S. Pei, X. Zhou, J. Chen, S. Wang, R. Zhao, W. Jiang, C. Liu, M. Huang, X. Wang, Y. Zhao, D. Yu, F. Ye, S. Wang, and J. Mei, Core-level x-ray photoemission and Raman spectroscopy studies on electronic structures in Mott-Hubbard type nickelate oxide NdNiO$_2$, arxiv:1911.03177.

[28] Q. Li, C. He, J. Si, X. Zhu, Y. Zhang, and H. H. Wen, Absence of superconductivity in bulk Nd$_{1-x}$Sr$_x$NiO$_2$, Commun. Mater. **1**, 16 (2020).

[29] X.-R. Zhou, Z.-X. Feng, P.-X. Qin, H. Yan, S. Hu, H.-X. Guo, X.-N. Wang, H.-J. Wu, X. Zhang, H.-Y. Chen, X.-P. Qiu, and Z.-Q. Liu, Absence of superconductivity in Nd$_{0.8}$Sr$_{0.2}$NiO$_x$ thin films without chemical reduction, Rare Met. Cement. Carbides **39**, 368 (2020).

[30] P. A. Lee, N. Nagaosa, and X. G. Wen, Doping a Mott insulator: Physics of high-temperature superconductivity, Rev. Mod. Phys. **78**, 17 (2006).

[31] H. Hosono and K. Kuroki, Iron-based superconductors: Current status of materials and pairing mechanism, Physica (Amsterdam) **514C**, 399 (2015).

[32] D. Li, B. Wang, K. Lee, Shannon P. Harvey, M. Osada, B. H. Goodge, L. F. Kourkoutis, and H. Y. Hwang, Super-conducting Dome in Nd$_{1-x}$Sr$_x$NiO$_2$ Infinite Layer Films, Phys. Rev. Lett. **125**, 027001 (2020).

[33] K. Lee, B. H. Goodge, D. Li, M. Osada, B. Y. Wang, Y. Cui, L. F. Kourkoutis, and H. Y. Hwang, Aspects of the synthesis of thin film superconducting infinite-layer nickelates, APL Mater. **8**, 041107 (2020).

[34] M. Kawai, S. Inoue, M. Mizumaki, N. Kawamura, N. Ichikawa, and Y. Shimakawa, Reversible changes of epitaxial thin films from perovskite LaNiO3 to infinite-layer structure LaNiO$_2$, Appl. Phys. Lett. **94**, 082102 (2009).

[35] M. A. Hayward, M. A. Green, M. J. Rosseinsky, and J. Sloan, Sodium hydride as a powerful reducing agent for topotactic oxide deintercalation-synthesis and characterization of the nickel(I) oxide LaNiO$_2$, J. Am. Chem. Soc. **121**, 8843 (1999).

[36] A. Ikeda, T. Manabe, and M. Naito, Comparison of reduction agents in the synthesis of infinite-layer LaNiO$_2$ films, Physica (Amsterdam) **506C**, 83 (2014).

[37] See Supplemental Material at http://link.aps.org/supplemental/10.1103/PhysRevLett.125.147003 for the following: Fig. S1 for XRD rocking curves of infinite-layer Nd$_{1-x}$Sr$_x$NiO$_2$ thin films; Fig. S2 for XRD θ-2θ scans of the as-grown Nd$_{1-x}$Sr$_x$NiO$_3$ thin films; Fig. S3 for ρ-T curves of a sample with $x = 0.2$ under various magnetic field; Fig. S4 for ρ-T curves of as-grown Nd$_{1-x}$Sr$_x$NiO$_3$ thin films; Fig. S5 for ρ-T curves of multiple samples for x from 0.12 to 0.3; Fig. S6 for the HAADF-STEM image of Nd$_{0.85}$Sr$_{0.15}$NiO$_2$ thin films; Fig. S7 for ρ-T curves of the ~10-nm Nd$_{1-x}$Sr$_x$NiO$_2$ thin films with $x = 0.15$ and $x = 0.2$; Fig. S8 for Hall resistances R_{xy} of Nd$_{1-x}$Sr$_x$NiO$_2$ thin films with $x = 0.15$ and $x = 0.2$.

[38] F. Rullier-Albenque, H. Alloul, and R. Tourbot, Disorder and Transport in Cuprates: Weak Localization and Magnetic Contributions, Phys. Rev. Lett. **87**, 157001 (2001).

[39] P. Fournier, J. Higgins, H. Balci, E. Maiser, C. J. Lobb, and R. L. Greene, Anomalous saturation of the phase coherence length in underdoped Pr$_{2-x}$Ce$_x$CuO$_4$ thin films, Phys. Rev. B **62**, R11993(R) (2000).

[40] Y. Dagan, M. M. Qazilbash, C. P. Hill, V. N. Kulkarni, and R. L. Greene, Evidence for a Quantum Phase Transition in Pr$_{2-x}$Ce$_x$CuO$_4$ from Transport Measurements, Phys. Rev. Lett. **92**, 167001 (2004).

[41] Y. Ando, Y. Kurita, S. Komiya, S. Ono, and K. Segawa, Evolution of the Hall Coefficient and the Peculiar Electronic Structure of the Cuprate Superconductors, Phys. Rev. Lett. **92**, 197001 (2004).

[42] H. Y. Hwang, B. Batlogg, H. Takagi, H. L. Kao, J. Kwo, R. J. Cava, J. J. Krajewski, and W. F. Peck, Jr., Scaling of the Temperature Dependent Hall Effect in La$_{2-x}$Sr$_x$CuO$_4$, Phys. Rev. Lett. **72**, 2636 (1994).

[43] L. Si, W. Xiao, J. Kaufmann, J. M. Tomczak, Y. Lu, Z. Zhong, and K. Held, Topotactic Hydrogen in Nickelate Superconductors and Akin Infinite-Layer Oxides ABO$_3$, Phys. Rev. Lett. **124**, 166402 (2020).

[44] Y. Krockenberger, J. Kurian, A. Winkler, A. Tsukada, M. Naito, and L. Alff, Superconductivity phase diagrams for the electron-doped cuprates R_{2-x}Ce$_x$CuO$_4$ (R = La, Pr, Nd, Sm, and Eu), Phys. Rev. B **77**, 060505(R) (2008).

[45] J. L. Peng, E. Maiser, T. Venkatesan, R. L. Greene, and G. Czjzek, Concentration range for superconductivity in high-quality Pr$_{2-x}$Ce$_x$CuO$_{4-y}$ thin films, Phys. Rev. B **55**, R6145 (1997).

[46] S. Karimoto, K. Ueda, M. Naito, and T. Imai, Single-crystalline superconducting thin films of electron-doped infinite-layer compounds grown by molecular-beam epitaxy, Appl. Phys. Lett. **79**, 2767 (2001).

[47] H. Takagi, T. Ido, S. Ishibashi, M. Uota, S. Uchida, and Y. Tokura, Superconductor-to-nonsuperconductor transition in (La$_{1-x}$Sr$_x$)$_2$CuO$_4$ as investigated by transport and magnetic measurements, Phys. Rev. B **40**, 2254 (1989).

[48] A. R. Moodenbaugh, Y. Xu, M. Suenaga, T. J. Folkerts, and R. N. Shelton, Superconducting properties of $La_{2-x}Ba_xCuO_4$, Phys. Rev. B **38**, 4596 (1988).

[49] J. S. Kim, S. S. A. Seo, M. F. Chisholm, R. Kremer, H.-U. Habermeier, B. Keimer, and H. N. Lee, Nonlinear Hall effect and multichannel conduction in $LaTiO_3/SrTiO_3$ superlattices, Phys. Rev. B **82**, 201407 (2010).

[50] R. Ohtsuka, M. Matvejeff, K. Nishio, R. Takahashi, and M. Lippmaa, Transport properties of $LaTiO_3/SrTiO_3$ heterostructures, Appl. Phys. Lett. **96**, 192111 (2010).